

Measurement of the Branching Ratios for the Decays of D_s^+ to $\eta\pi^+$, $\eta'\pi^+$, $\eta\rho^+$, and $\eta'\rho^+$

CLEO Collaboration

(January 1, 2018)

Abstract

Using a data sample with integrated luminosity of 3.9 fb^{-1} collected in e^+e^- annihilation with the CLEO-II detector at the Cornell Electron Storage Ring, we have measured the branching ratios for the decay modes $D_s^+ \rightarrow (\eta, \eta')\pi^+$ and $D_s^+ \rightarrow (\eta, \eta')\rho^+$ relative to $D_s^+ \rightarrow \phi\pi^+$. These decay modes are among the most common hadronic decays of the D_s^+ , and can be related by factorization to the semileptonic decays $D_s^+ \rightarrow (\eta, \eta')\ell^+\nu_\ell$. The results obtained are compared with previous CLEO results and with the branching ratios measured for the related semileptonic decays. We also report results on the Cabibbo-suppressed decays of the D^+ to the same final states.

C. P. Jessop,¹ K. Lingel,¹ H. Marsiske,¹ M. L. Perl,¹ S. F. Schaffner,¹ D. Ugolini,¹
 R. Wang,¹ X. Zhou,¹ T. E. Coan,² V. Fadeyev,² I. Korolkov,² Y. Maravin,² I. Narsky,²
 V. Shelkov,² J. Staeck,² R. Stroynowski,² I. Volobouev,² J. Ye,² M. Artuso,³ A. Efimov,³
 F. Frascioni,³ M. Gao,³ M. Goldberg,³ D. He,³ S. Kopp,³ G. C. Moneti,³ R. Mountain,³
 Y. Mukhin,³ S. Schuh,³ T. Skwarnicki,³ S. Stone,³ G. Viehhauser,³ X. Xing,³ J. Bartelt,⁴
 S. E. Csorna,⁴ V. Jain,⁴ S. Marka,⁴ A. Freyberger,⁵ R. Godang,⁵ K. Kinoshita,⁵ I. C. Lai,⁵
 P. Pomianowski,⁵ S. Schrenk,⁵ G. Bonvicini,⁶ D. Cinabro,⁶ R. Greene,⁶ L. P. Perera,⁶
 B. Barish,⁷ M. Chadha,⁷ S. Chan,⁷ G. Eigen,⁷ J. S. Miller,⁷ C. O'Grady,⁷ M. Schmidtler,⁷
 J. Urheim,⁷ A. J. Weinstein,⁷ F. Würthwein,⁷ D. M. Asner,⁸ D. W. Bliss,⁸ W. S. Brower,⁸
 G. Masek,⁸ H. P. Paar,⁸ V. Sharma,⁸ J. Gronberg,⁹ R. Kutschke,⁹ D. J. Lange,⁹
 S. Menary,⁹ R. J. Morrison,⁹ H. N. Nelson,⁹ T. K. Nelson,⁹ C. Qiao,⁹ J. D. Richman,⁹
 D. Roberts,⁹ A. Ryd,⁹ M. S. Witherell,⁹ R. Balest,¹⁰ B. H. Behrens,¹⁰ K. Cho,¹⁰
 W. T. Ford,¹⁰ H. Park,¹⁰ P. Rankin,¹⁰ J. Roy,¹⁰ J. G. Smith,¹⁰ J. P. Alexander,¹¹
 C. Bebek,¹¹ B. E. Berger,¹¹ K. Berkelman,¹¹ K. Bloom,¹¹ D. G. Cassel,¹¹ H. A. Cho,¹¹
 D. M. Coffman,¹¹ D. S. Crowcroft,¹¹ M. Dickson,¹¹ P. S. Drell,¹¹ K. M. Ecklund,¹¹
 R. Ehrlich,¹¹ R. Elia,¹¹ A. D. Foland,¹¹ P. Gaidarev,¹¹ B. Gittelman,¹¹ S. W. Gray,¹¹
 D. L. Hartill,¹¹ B. K. Heltsley,¹¹ P. I. Hopman,¹¹ J. Kandaswamy,¹¹ N. Katayama,¹¹
 P. C. Kim,¹¹ D. L. Kreinick,¹¹ T. Lee,¹¹ Y. Liu,¹¹ G. S. Ludwig,¹¹ J. Masui,¹¹
 J. Mevissen,¹¹ N. B. Mistry,¹¹ C. R. Ng,¹¹ E. Nordberg,¹¹ M. Ogg,^{11,*} J. R. Patterson,¹¹
 D. Peterson,¹¹ D. Riley,¹¹ A. Soffer,¹¹ C. Ward,¹¹ M. Athanas,¹² P. Avery,¹² C. D. Jones,¹²
 M. Lohner,¹² C. Prescott,¹² S. Yang,¹² J. Yelton,¹² J. Zheng,¹² G. Brandenburg,¹³
 R. A. Briere,¹³ Y.S. Gao,¹³ D. Y.-J. Kim,¹³ R. Wilson,¹³ H. Yamamoto,¹³ T. E. Browder,¹⁴
 F. Li,¹⁴ Y. Li,¹⁴ J. L. Rodriguez,¹⁴ T. Bergfeld,¹⁵ B. I. Eisenstein,¹⁵ J. Ernst,¹⁵
 G. E. Gladding,¹⁵ G. D. Gollin,¹⁵ R. M. Hans,¹⁵ E. Johnson,¹⁵ I. Karliner,¹⁵ M. A. Marsh,¹⁵
 M. Palmer,¹⁵ M. Selen,¹⁵ J. J. Thaler,¹⁵ K. W. Edwards,¹⁶ A. Bellerive,¹⁷ R. Janicek,¹⁷
 D. B. MacFarlane,¹⁷ K. W. McLean,¹⁷ P. M. Patel,¹⁷ A. J. Sadoff,¹⁸ R. Ammar,¹⁹
 P. Baringer,¹⁹ A. Bean,¹⁹ D. Besson,¹⁹ D. Coppage,¹⁹ C. Darling,¹⁹ R. Davis,¹⁹
 N. Hancock,¹⁹ S. Kotov,¹⁹ I. Kravchenko,¹⁹ N. Kwak,¹⁹ S. Anderson,²⁰ Y. Kubota,²⁰
 M. Lattery,²⁰ J. J. O'Neill,²⁰ S. Patton,²⁰ R. Poling,²⁰ T. Riehle,²⁰ V. Savinov,²⁰ A. Smith,²⁰
 M. S. Alam,²¹ S. B. Athar,²¹ Z. Ling,²¹ A. H. Mahmood,²¹ H. Severini,²¹ S. Timm,²¹
 F. Wappler,²¹ A. Anastassov,²² S. Blinov,^{22,†} J. E. Duboscq,²² K. D. Fisher,²² D. Fujino,^{22,‡}
 R. Fulton,²² K. K. Gan,²² T. Hart,²² K. Honscheid,²² H. Kagan,²² R. Kass,²² J. Lee,²²
 M. B. Spencer,²² M. Sung,²² A. Undrus,^{22,†} R. Wanke,²² A. Wolf,²² M. M. Zoeller,²²
 B. Nemati,²³ S. J. Richichi,²³ W. R. Ross,²³ P. Skubic,²³ M. Wood,²³ M. Bishai,²⁴ J. Fast,²⁴
 E. Gerndt,²⁴ J. W. Hinson,²⁴ N. Menon,²⁴ D. H. Miller,²⁴ E. I. Shibata,²⁴ I. P. J. Shipsey,²⁴
 M. Yurko,²⁴ L. Gibbons,²⁵ S. D. Johnson,²⁵ Y. Kwon,²⁵ S. Roberts,²⁵ and E. H. Thorndike²⁵

¹Stanford Linear Accelerator Center, Stanford University, Stanford, California 94309

*Permanent address: University of Texas, Austin TX 78712

†Permanent address: BINP, RU-630090 Novosibirsk, Russia.

‡Permanent address: Lawrence Livermore National Laboratory, Livermore, CA 94551.

- ²Southern Methodist University, Dallas, Texas 75275
- ³Syracuse University, Syracuse, New York 13244
- ⁴Vanderbilt University, Nashville, Tennessee 37235
- ⁵Virginia Polytechnic Institute and State University, Blacksburg, Virginia 24061
- ⁶Wayne State University, Detroit, Michigan 48202
- ⁷California Institute of Technology, Pasadena, California 91125
- ⁸University of California, San Diego, La Jolla, California 92093
- ⁹University of California, Santa Barbara, California 93106
- ¹⁰University of Colorado, Boulder, Colorado 80309-0390
- ¹¹Cornell University, Ithaca, New York 14853
- ¹²University of Florida, Gainesville, Florida 32611
- ¹³Harvard University, Cambridge, Massachusetts 02138
- ¹⁴University of Hawaii at Manoa, Honolulu, Hawaii 96822
- ¹⁵University of Illinois, Champaign-Urbana, Illinois 61801
- ¹⁶Carleton University, Ottawa, Ontario, Canada K1S 5B6
and the Institute of Particle Physics, Canada
- ¹⁷McGill University, Montréal, Québec, Canada H3A 2T8
and the Institute of Particle Physics, Canada
- ¹⁸Ithaca College, Ithaca, New York 14850
- ¹⁹University of Kansas, Lawrence, Kansas 66045
- ²⁰University of Minnesota, Minneapolis, Minnesota 55455
- ²¹State University of New York at Albany, Albany, New York 12222
- ²²Ohio State University, Columbus, Ohio 43210
- ²³University of Oklahoma, Norman, Oklahoma 73019
- ²⁴Purdue University, West Lafayette, Indiana 47907
- ²⁵University of Rochester, Rochester, New York 14627

I. INTRODUCTION

Among the most common hadronic decay modes for the D_s^+ are the decays $D_s^+ \rightarrow (\eta, \eta')\pi^+$ and $D_s^+ \rightarrow (\eta, \eta')\rho^+$, where the notation $D_s^+ \rightarrow (\eta, \eta')\pi^+$ represents the decays $D_s^+ \rightarrow \eta\pi^+$ and $D_s^+ \rightarrow \eta'\pi^+$. As can be seen from Figure 1, they are related by factorization to the semileptonic decays $D_s^+ \rightarrow (\eta, \eta')\ell^+\nu_\ell$. This relation has been extensively discussed by Kamal, Xu, and Czarnecki [1]. One prediction of the factorization hypothesis is that the D_s^+ decay rate to $\eta\rho^+$ can be simply related to the corresponding semileptonic decay rate evaluated at $q^2 = m_\rho^2$:

$$\Gamma(D_s^+ \rightarrow \eta\rho^+) = 6\pi^2 a_1^2 f_\rho^2 |V_{ud}|^2 \frac{d\Gamma}{dq^2}(D_s^+ \rightarrow \eta\ell^+\nu_\ell)|_{(q^2=m_\rho^2)}. \quad (1)$$

Here f_ρ is the decay constant for the ρ and a_1 is a strong interaction coefficient that is measured in two-body hadronic D^0 decays.

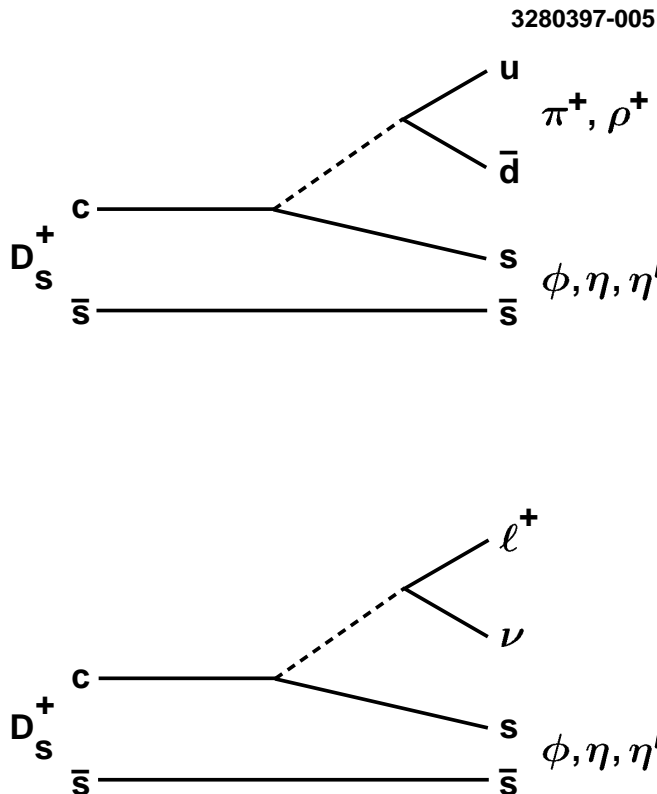


FIG. 1. Related Feynman diagrams for hadronic and semileptonic D_s^+ decays

To test this factorization prediction experimentally, a shape for the form factor must be assumed. It is expected to be very close to the form factor for $D^0 \rightarrow K^- e^+ \nu_e$, for which

$$\frac{\Gamma(D^0 \rightarrow K^- e^+ \nu_e)}{d\Gamma(D^0 \rightarrow K^- e^+ \nu_e)/dq^2|_{(q^2=m_\rho^2)}} = 1.30 \pm 0.01 \text{ GeV}^2.$$

This number is calculated using the CLEO measurement of the form factor [2]. Assuming a similar pole shape for the D_s^+ form factor yields the prediction $\Gamma(D_s^+ \rightarrow \eta\rho^+)/\Gamma(D_s^+ \rightarrow \eta e^+\nu_e) \approx 2.9$ and $\Gamma(D_s^+ \rightarrow \eta'\rho^+)/\Gamma(D_s^+ \rightarrow \eta' e^+\nu_e) \approx 2.9$ [3].

In 1992 CLEO [4] measured the branching ratios for the hadronic modes studied here using a much smaller data sample of 0.69 fb^{-1} . Combining these measurements with the more recent CLEO measurements of the semileptonic modes [5], we calculate the $\Gamma(D_s^+ \rightarrow \eta\rho^+)/\Gamma(D_s^+ \rightarrow \eta e^+\nu_e) = 4.3 \pm 1.1$ and $\Gamma(D_s^+ \rightarrow \eta'\rho^+)/\Gamma(D_s^+ \rightarrow \eta' e^+\nu_e) = 14.8 \pm 5.8$. The last number is well above the factorization prediction of 2.9. Theoretical efforts to understand charm nonleptonic decays, even including final state interactions, cannot account for the very large branching ratio for $D_s^+ \rightarrow \eta'\rho^+$ [9,10].

Because of the interest in these branching fractions, we have remeasured them using the much larger data sample now available. In the present analysis we use data corresponding to an integrated luminosity of 3.9 fb^{-1} (which includes the 0.69 fb^{-1} used in the previous analysis) to remeasure the four modes, $D_s^+ \rightarrow (\eta, \eta')\pi^+$ and $D_s^+ \rightarrow (\eta, \eta')\rho^+$. The data were collected with the CLEO II detector at the Cornell Electron Storage Ring (CESR), at center-of-mass energies equal to the mass of the $\Upsilon(4S)$ and in the continuum just below the $\Upsilon(4S)$ resonance.

The CLEO-II detector is designed to detect both charged and neutral particles with high resolution and efficiency. The detector consists of a charged-particle tracking system surrounded by a time-of-flight scintillator system. These are in turn surrounded by an electromagnetic calorimeter which consists of 7800 thallium-doped CsI crystals. This inner detector is immersed in a 1.5 T solenoidal magnetic field generated by a superconducting coil. Muon detection is achieved using proportional tubes interleaved with iron. A more complete description of the detector can be found elsewhere [6].

II. EVENT SELECTION

All events in this analysis are required to pass standard CLEO criteria for hadronic events. Since all the signal modes involve only pions in the final state, systematic errors are reduced by imposing no hadron identification cuts on either signal modes or the normalization mode. All D_s^+ candidates are required to have $x = P_{D_s}/P_{max} > 0.63$ ($P_{max}^2 = E_{beam}^2 - M_{D_s}^2$) to suppress combinatoric background. Throughout this paper, reference to a particular charge state implies the inclusion of the charge-conjugate state as well.

All photons are required to be in the good barrel region of the calorimeter ($|\cos\theta| < 0.71$), to have a minimum energy of 30 MeV, and to not match the projection of a charged track. We choose pairs of photons whose invariant mass is within $2.5\sigma(M)$ of the nominal π^0 mass; $\sigma(M)$ is approximately $6 \text{ MeV}/c^2$. We then kinematically constrain the $\gamma\gamma$ pairs to the nominal π^0 mass in order to improve the momentum resolution of the π^0 . We also require that $|\cos\theta_{\pi^0}| < 0.8$, where θ_{π^0} is the angle between one γ in the π^0 rest frame and the π^0 momentum in the lab frame. The signal is flat in $|\cos\theta_{\pi^0}|$ and the background peaks toward +1.

For $\eta \rightarrow \gamma\gamma$ decays, the η is selected in a manner similar to the π^0 , but with the additional constraint that photons which could be paired to make π^0 's with momentum greater than $0.8 \text{ GeV}/c$ are rejected. We also detect η 's using the $\eta \rightarrow \pi^+\pi^-\pi^0$ decay chain, although

this mode gives a sample with fewer events and less significance than the two-photon decay mode. A π^0 momentum greater than 0.4 GeV/c is required. All η candidates within $2.5\sigma(M)$ of the nominal mass are considered, where $\sigma(M)$ is the r.m.s. mass resolution for the given mode, typically about 14 MeV/c² for the $\gamma\gamma$ mode, and 6 MeV/c² for the $\pi^+\pi^-\pi^0$ mode. In order to improve the momentum resolution of the η , the decay particles from the η are kinematically constrained to the nominal η mass.

To select η' candidates we use the $\eta\pi^+\pi^-$ final state, where the η is detected in both $\gamma\gamma$ and $\pi^+\pi^-\pi^0$ modes. Both η and η' candidates are kinematically constrained to the nominal mass in order to improve the momentum resolution.

Reconstruction efficiencies and invariant mass resolutions were determined by using a GEANT-based [7] Monte Carlo (MC) simulation of the detector.

III. D_s^+ DECAYS INTO MODES CONTAINING A π^+

Five modes are studied in which a pion is produced in the weak decay:

1. $D_s^+ \rightarrow \phi\pi^+$ (the normalization mode), $\phi \rightarrow K^+K^-$
2. $D_s^+ \rightarrow \eta\pi^+$, $\eta \rightarrow \gamma\gamma$
3. $D_s^+ \rightarrow \eta\pi^+$, $\eta \rightarrow \pi^+\pi^-\pi^0$
4. $D_s^+ \rightarrow \eta'\pi^+$, $\eta' \rightarrow \eta\pi^+\pi^-$, $\eta \rightarrow \gamma\gamma$
5. $D_s^+ \rightarrow \eta'\pi^+$, $\eta' \rightarrow \eta\pi^+\pi^-$, $\eta \rightarrow \pi^+\pi^-\pi^0$

We require the pions that come directly from the weak decay to have momentum greater than 0.7 GeV/c and the η or η' from the D_s^+ to have momentum greater than 1 GeV/c. This reduces the background from random combinations.

A. $D_s^+ \rightarrow \phi\pi^+$

Since this decay involves a pseudoscalar meson decaying into a vector meson and a pseudoscalar π^+ , the ϕ must be polarized in the helicity zero state. We take advantage of this by cutting on $\cos\theta_{K^+}$, where θ_{K^+} is the angle between the K^+ momentum and the direction opposite to the D_s^+ momentum in the ϕ rest frame. The angle is shown in Figure 2. The signal has a $\cos^2\theta_{K^+}$ distribution, while the background is flat in $\cos\theta_{K^+}$. We require $|\cos\theta_{K^+}| > 0.45$.

We select ϕ mesons within ± 8 MeV of the peak mass, and form the $\phi\pi^+$ mass spectrum shown in Figure 3. The $\phi\pi^+$ mass distribution shows two clear peaks, one from the D_s^+ and the other from the D^+ . To fit the spectrum we use four functions:

1. The D_s^+ signal is fit to a sum of two Gaussians with a common mean; the widths and relative areas are fixed to values determined from the Monte-Carlo signal simulation. The mean is allowed to vary in the fit.

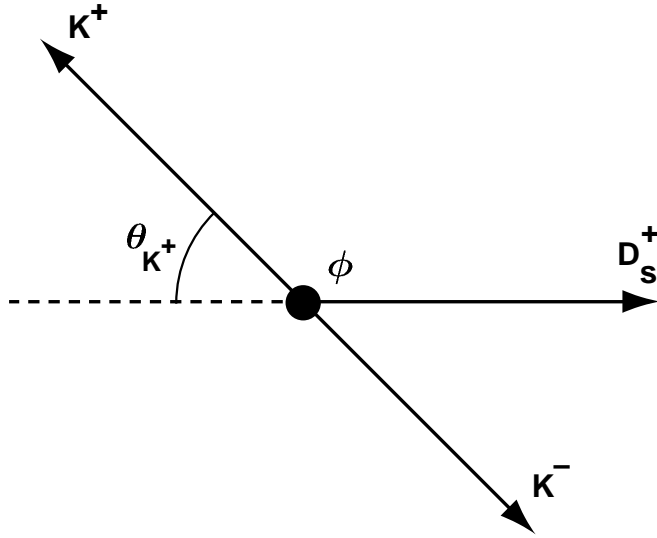


FIG. 2. Illustration of the helicity angle, θ_{K^+} . All vectors represent momenta in the ϕ rest frame.

2. The D^+ signal shape is of the same form as for the D_s^+ , with the mass constrained to be $0.099 \text{ GeV}/c^2$ less than the D_s^+ mass, which is the precisely measured mass difference [8].
3. The shape of the function used to represent the $D_s^+ \rightarrow (\phi, \eta, \eta')\rho^+$ feed-through is determined from Monte Carlo. This feed-through causes a broad peak in the mass of the $(\phi, \eta, \eta')\pi^+$ system centered at $1.7 \text{ GeV}/c^2$, which is parameterized with a Gaussian. The normalization of the feed-through is determined from the measurement of the branching ratio [4].
4. A second-order Chebyshev polynomial is used to represent the combinatoric background.

This fit yields $3748 \pm 91 D_s^+$ events. In all other fits, four functions are also used, although the combinatoric background shape depends on the particular mode.

B. $D_s^+ \rightarrow \eta\pi^+$

In Figure 4 we show the $\eta\pi^+$ invariant mass spectrum for both decay modes of the η . The signal peaks are evident for both the D_s^+ and D^+ . The peak at the D_s^+ contains 766 ± 44 events for the channel $\eta \rightarrow \gamma\gamma$, and 154 ± 22 events for the channel $\eta \rightarrow \pi^+\pi^-\pi^0$. Multiple entries into the plot from a single event are allowed, and no effort is made to select among them. In Table I we list the yields for different channels and their efficiencies for D_s^+ decay. We also list the measurement for the ratio $\Gamma(D_s^+ \rightarrow \eta_{\gamma\gamma}\pi^+)/\Gamma(D_s^+ \rightarrow \phi\pi^+)$. In the table ϵ is the efficiency and ϵB is efficiency multiplied by branching fraction of the secondary decays. The systematic errors for the efficiencies relative to the $\phi\pi^+$ mode have several sources and differ slightly from mode to mode. For the $\eta_{\gamma\gamma}\pi^+$ mode the systematic error includes

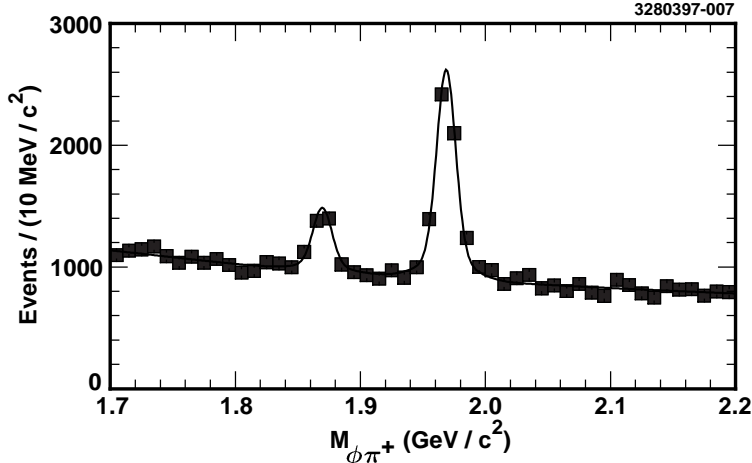


FIG. 3. The $M(\phi\pi^+)$ distribution. The larger peak is due to the decay $D_s^+ \rightarrow \phi\pi^+$; the smaller peak at lower mass is due to $D^+ \rightarrow \phi\pi^+$.

uncertainties in the relative charged track (4%) and photon detection efficiencies (5%). We studied the Monte Carlo shape by letting the width of the two Gaussians vary in the fit and then calculated the shift in the central value, giving us an uncertainty of 3%. We also used different background shapes to determine the uncertainty due to the unknown background shape, and obtained an error of 4%. The total systematic error obtained by adding these uncorrelated errors in quadrature is 8%. For the $\eta_{3\pi}\pi^+$ mode the systematic error includes uncertainties in the photon detection efficiency (5%) and in the signal (5%) and background (8%) shapes. In addition there was a systematic error of (10%) due to the modeling of multiple entries. The total systematic error obtained by adding these uncorrelated errors in quadrature is 15%.

TABLE I. Fit Results for $D_s^+ \rightarrow (\eta, \eta')\pi^+$. BR is the branching ratio of the $\phi(\eta, \eta')$ decay mode that is used.

Mode	N	$\epsilon(\%)$	$\epsilon B(\%)$	$\Gamma/\Gamma(\phi\pi)$
$\phi\pi$	3748 ± 91	19.1 ± 0.2	9.4	
$\eta_{\gamma\gamma}\pi$	766 ± 44	9.6 ± 0.1	3.7	$0.52 \pm 0.03 \pm 0.04$
$\eta_{3\pi}\pi$	154 ± 22	4.5 ± 0.1	1.1	$0.35 \pm 0.05 \pm 0.06$
$\eta'(\eta_{\gamma\gamma})\pi$	479 ± 26	6.7 ± 0.1	1.1	$1.09 \pm 0.06 \pm 0.07$
$\eta'(\eta_{3\pi})\pi$	58 ± 9	1.9 ± 0.1	0.2	$0.73 \pm 0.11 \pm 0.12$

The measured ratio for $\Gamma(D_s^+ \rightarrow \eta_{3\pi}\pi^+)/\Gamma(D_s^+ \rightarrow \phi\pi^+)$ shown in Table I is approximately two standard deviations lower than the corresponding ratio for the $\eta_{\gamma\gamma}$ mode, taking into account the systematic errors which are not in common to the two modes. The measurements of $D_s^+ \rightarrow \eta'\pi^+$, described in the next section, show a similar discrepancy, as do the $D^+ \rightarrow \eta\pi^+$ and $\eta'\pi^+$, although those have less statistical significance. As a result, we searched in some detail for a systematic discrepancy in reconstructing the two η decay modes. To calibrate the relative efficiency for these modes, and to check the reconstruction program, we studied events of the type $D^{*+} \rightarrow D^0\pi^+$ with $D^0 \rightarrow \bar{K}^{*0}\eta$. This has a very large and clean signal, and an η momentum spectrum very similar to that for the D_s^+ decays. Using this process,

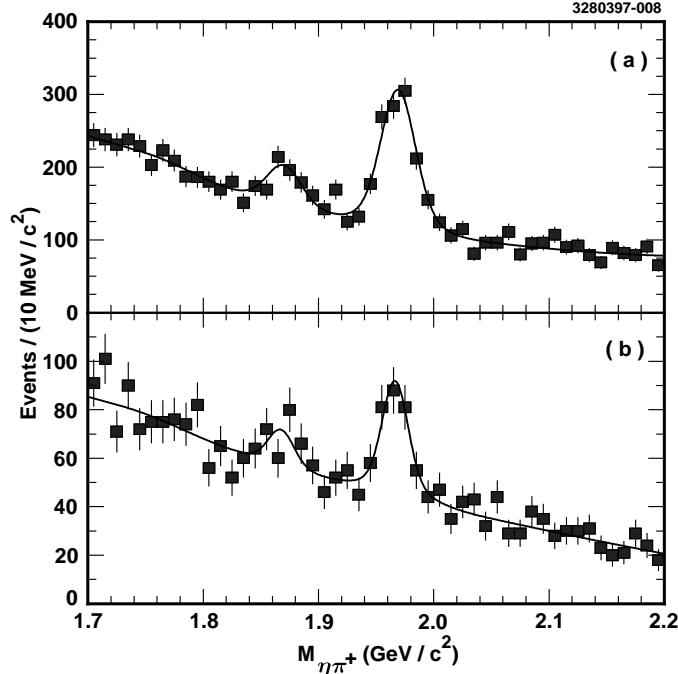


FIG. 4. The $M(\eta\pi^+)$ distribution for (a) $\eta \rightarrow \gamma\gamma$, (b) $\eta \rightarrow \pi^+\pi^-\pi^0$.

TABLE II. Fit Results for $D^+ \rightarrow (\eta, \eta')\pi^+$.

Mode	N	$\epsilon(\%)$	$\epsilon B(\%)$	$\Gamma/\Gamma(\phi\pi)$
$\phi\pi$	1133 ± 72	20.3 ± 0.2	9.9	
$\eta_{\gamma\gamma}\pi$	225 ± 38	9.6 ± 0.2	3.7	$0.53 \pm 0.09 \pm 0.05$
$\eta_{3\pi}\pi$	50 ± 20	4.6 ± 0.1	1.1	$0.40 \pm 0.15 \pm 0.07$
$\eta'(\eta_{\gamma\gamma})\pi$	114 ± 18	6.8 ± 0.1	1.1	$0.90 \pm 0.14 \pm 0.07$
$\eta'(\eta_{3\pi})\pi$	12 ± 7	1.9 ± 0.1	0.2	$0.52 \pm 0.29 \pm 0.09$

we measure $B(\eta \rightarrow \gamma\gamma)/B(\eta \rightarrow \pi^+\pi^-\pi^0) = 1.53 \pm 0.16 \pm 0.10$, compared to the PDG value of 1.64 ± 0.04 [8]. This confirms that the relative efficiency for the two decay modes of the η is reproduced properly in the Monte Carlo simulation. Other checks using the data also reproduced the expected ratio of $B(\eta \rightarrow \gamma\gamma)/B(\eta \rightarrow \pi^+\pi^-\pi^0)$, although with limited statistical power. Since we were unable to isolate any systematic effect, we attribute the difference between the two $D_s^+ \rightarrow \eta\pi^+$ measurements to an unlikely set of statistical fluctuations.

The yields and relative branching ratios for all of the D^+ decays into the same final states are shown in Table II. The efficiencies for the D^+ modes are generally very close to those for the corresponding D_s^+ decays.

C. $D_s^+ \rightarrow \eta'\pi^+$

For this mode, we can apply cuts on both the η mass and the η' mass, reducing the background substantially. Each mass provides a kinematic constraint, helping to improve

the resolution for the $\eta'\pi^+$ mass. As a result, these modes are significantly cleaner than $D_s^+ \rightarrow \eta\pi^+$. We require the momentum of the η' to be greater than 1.0 GeV/c.

In Figure 5 we show the $\eta'\pi^+$ invariant mass spectrum for both η decay modes. The peak at the D_s^+ mass contains 479 ± 26 events for the channel $\eta \rightarrow \gamma\gamma$, and 58 ± 9 events for the channel $\eta \rightarrow \pi^+\pi^-\pi^0$. The efficiencies and relative branching ratios are shown in Table I. The systematic error on the branching ratio measurement due to the uncertainty in charged track efficiency is negligible for the case of $\eta \rightarrow \gamma\gamma$ because the final state has the same number of charged tracks as the normalizing mode. The main contributions to the systematic error are the uncertainties in the photon detection efficiency (5%) and in the shapes used to describe signal (3%) and background (3%). The total systematic error obtained by adding these uncorrelated errors in quadrature is 6%. For the channel $\eta \rightarrow \pi^+\pi^-\pi^0$, the main contributions to the systematic error are the uncertainties in the efficiency for charged tracks (4%) and photons (5%) and in the shapes for signal (10%) and background (4%), and in handling of multiple entries (10%). The total systematic error obtained by adding these uncorrelated errors in quadrature is 16%.

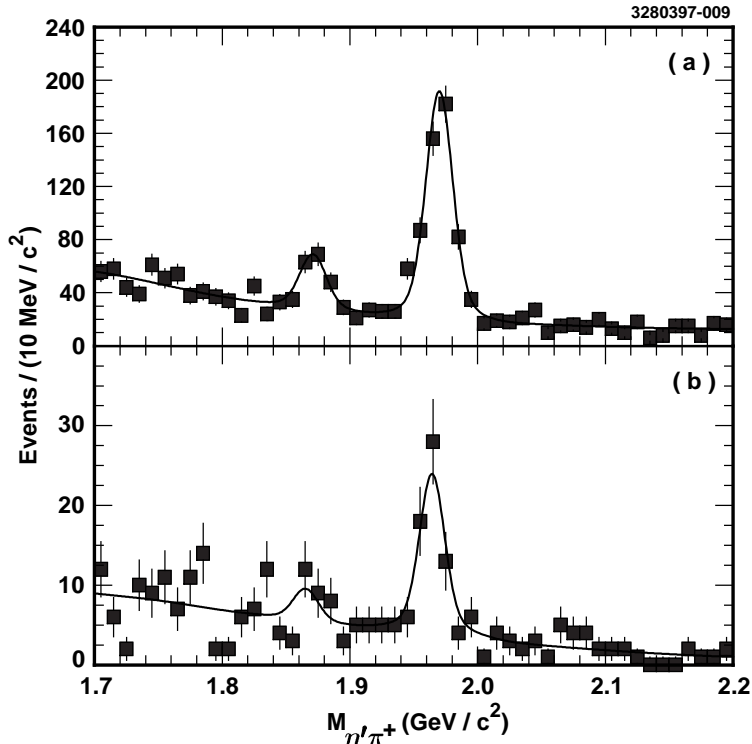


FIG. 5. The $M(\eta'\pi^+)$ distribution, using the decay mode $\eta' \rightarrow \eta\pi^+\pi^-$ with (a) $\eta \rightarrow \gamma\gamma$, (b) $\eta \rightarrow \pi^+\pi^-\pi^0$.

In $D_s^+ \rightarrow \eta'\pi^+$, $\eta' \rightarrow \eta\pi^+\pi^-$, $\eta \rightarrow \pi^+\pi^-\pi^0$, we found that there are many events with multiple combinations of pions which satisfy our selection criteria. Most of them come from real η' decays in which different rearrangements of the same four charged pions (two directly from the η' and two from the η), plus the π^0 , pass our η and η' cuts. We take only one candidate per event, choosing the candidate with the minimum value of a χ^2 based on the π^0 , η , and η' masses: $\chi^2 = \frac{(\delta M_{\eta'})^2}{\sigma_{\eta'}^2} + \frac{(\delta M_{\eta})^2}{\sigma_{\eta}^2} + \frac{(\delta M_{\pi^0})^2}{\sigma_{\pi^0}^2}$. The resulting measurements are shown

in Tables I and II.

IV. D_s^+ DECAYS INTO MODES CONTAINING A ρ^+

The analogous D_s^+ decay channels, where the π^+ has been replaced by a ρ^+ , can be studied using very similar cuts. Because of lower rates, lower efficiency, and a serious problem with multiple combinations within the same event, the $\eta \rightarrow \pi^+\pi^-\pi^0$ decay does not add significantly to the measurements of these modes, and is not used. A data sample with about 20% less integrated luminosity was used for the measurements of these modes.

A. $D_s^+ \rightarrow \eta\rho^+$

For the decay mode $D_s^+ \rightarrow \eta\rho^+$, we need to consider the possibility of nonresonant $\eta\pi^+\pi^0$ feedthrough. For Figure 6, we require the helicity angle to be in the range $|\cos\theta_{\pi^+}| > 0.45$, and the invariant mass of the $\pi^+\pi^0$ to be within ± 170 MeV/ c^2 of the ρ^+ mass. A fit to the resulting $\eta\pi^+\pi^0$ mass spectrum is shown, yielding 589 ± 43 $D_s^+ \rightarrow \eta\rho^+$ candidates and 8 ± 32 $D^+ \rightarrow \eta\rho^+$ candidates; thus there is no evidence of $D^+ \rightarrow \eta\rho^+$. We cannot directly extract a branching ratio for $D_s^+ \rightarrow \eta\rho^+$, however, until we account for possible nonresonant feedthrough.

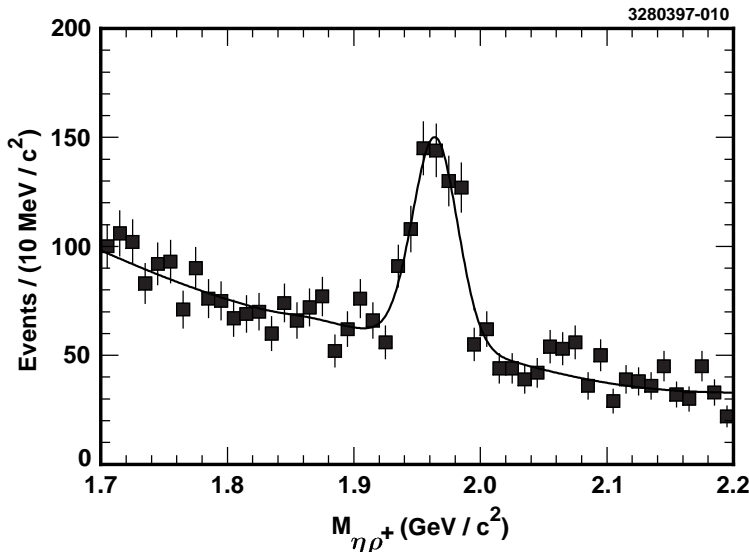


FIG. 6. The $M(\eta\rho^+)$ distribution, with $\eta \rightarrow \gamma\gamma$.

Although cuts on the helicity angle and on the ρ mass region can be used, the most reliable way to measure the resonant branching ratio is to fit the Dalitz plot. By doing this we make full use of the di-pion mass and the helicity angle to isolate the $\eta\rho^+$ signal. We therefore make a Dalitz plot of all events with $1.94 < M(\eta\pi^+\pi^0) < 1.99$ GeV/ c^2 , removing the cuts on helicity angle and on the $\pi^+\pi^0$ mass. In Figure 7 we show four Dalitz plots: (a) the signal region in the data, defined as $1.94 < M(\eta\pi^+\pi^0) < 1.99$ GeV/ c^2 ; (b) the M_{D_s} data sidebands, which are the mass regions $1.75 < M(\eta\pi^+\pi^0) < 1.90$ GeV/ c^2 and

$2.04 < M(\eta\pi^+\pi^0) < 2.24$ GeV/ c^2 ; (c) the full Monte Carlo of the $\eta\rho^+$ signal; and (d) a simulation using a parameterized Monte Carlo of nonresonant $\eta\pi^+\pi^0$ events generated according to phase space.

We do not expect $\eta\pi$ resonant structures in this Dalitz plot because isospin forbids $s\bar{s} \rightarrow \eta\pi$. For all four Dalitz plots, we recalculate the values of $M^2(\eta\pi^+)$ and $M^2(\pi^+\pi^0)$ so that the Dalitz boundary corresponds exactly to that of the mass of the D_s^+ [8], giving the sidebands the same boundary as the signal region. This causes negligible smearing of the ρ^+ resonance.

The most obvious feature of the Dalitz plot is that the ρ^+ region stands out so clearly in the data, even though there is a significant non- D_s^+ background which contains very little ρ^+ . A binned Dalitz fit to the data distribution in the signal region was performed using the sum of the distributions in the other three plots in Figure 7. The normalization of the non- D_s^+ component is fixed using a fit to the $\eta\rho^+$ mass distribution as in Figure 6 but without helicity angle and ρ mass cuts. The number of the resonant and nonresonant D_s^+ events is varied in the fit, with no interference term allowed. The results of the fit are shown in Table III. The systematic error includes uncertainties in the efficiencies for charged tracks (4%) and photons (10%) and the shapes for the signal (4%) and the background (3%).

In order to understand the systematic error due to possible interference between the resonant and nonresonant decays we also did a coherent Dalitz fit. The density of the events in the Dalitz plot is represented by the expression

$$I = A_1^2 + A_2^2 + B \times 2A_1A_2 \cos(\delta_1 - \delta_2),$$

where A_1 and δ_1 are the amplitude and phase of the Breit-Wigner resonance, A_2 and δ_2 are the amplitude and phase of the nonresonant decay, both of which are assumed to be constant, and B is an additional constant which is allowed to vary from zero to one. The case $B = 0$ corresponds to no interference between the resonant and the nonresonant part; the case $B = 1$ corresponds to full interference, expected if the nonresonant case were indeed a single partial wave with constant phase. The true case could lie anywhere between these two limits. In the fit when the constant B is allowed to float it takes the value 0.24 ± 0.20 , consistent with no interference. We therefore use the result from the incoherent fit to determine the branching ratio, and use the result from the coherent fit with $B = 0.44$ to find a conservative systematic error from this source. This corresponds to a 3.6% error. The total systematic error, obtained by adding this error in quadrature with the other systematic errors mentioned above, is estimated to be 12%.

B. $D_s^+ \rightarrow \eta'\rho^+$

The decay $D_s^+ \rightarrow \eta'\rho^+$ was reconstructed using the decay mode $\eta' \rightarrow \eta\pi^+\pi^-$, with $\eta \rightarrow \gamma\gamma$. We require the momentum of the η' to be greater than 1.0 GeV/ c and the invariant mass of the two pions to be within ± 170 MeV of the ρ^+ mass. In Figure 8 we can see a clear peak of $M_{\eta'\pi^+\pi^0}$. The fit yields 181 ± 18 $D_s^+ \rightarrow \eta'\rho^+$ events and -4 ± 10 $D^+ \rightarrow \eta'\rho^+$ events; thus there is no evidence for $D^+ \rightarrow \eta'\rho^+$.

As for the case of the $\eta\rho^+$ decay mode, we need to subtract any nonresonant feedthrough into the $\eta'\rho^+$ final state. In this case, however, a Dalitz plot is not as useful in separating

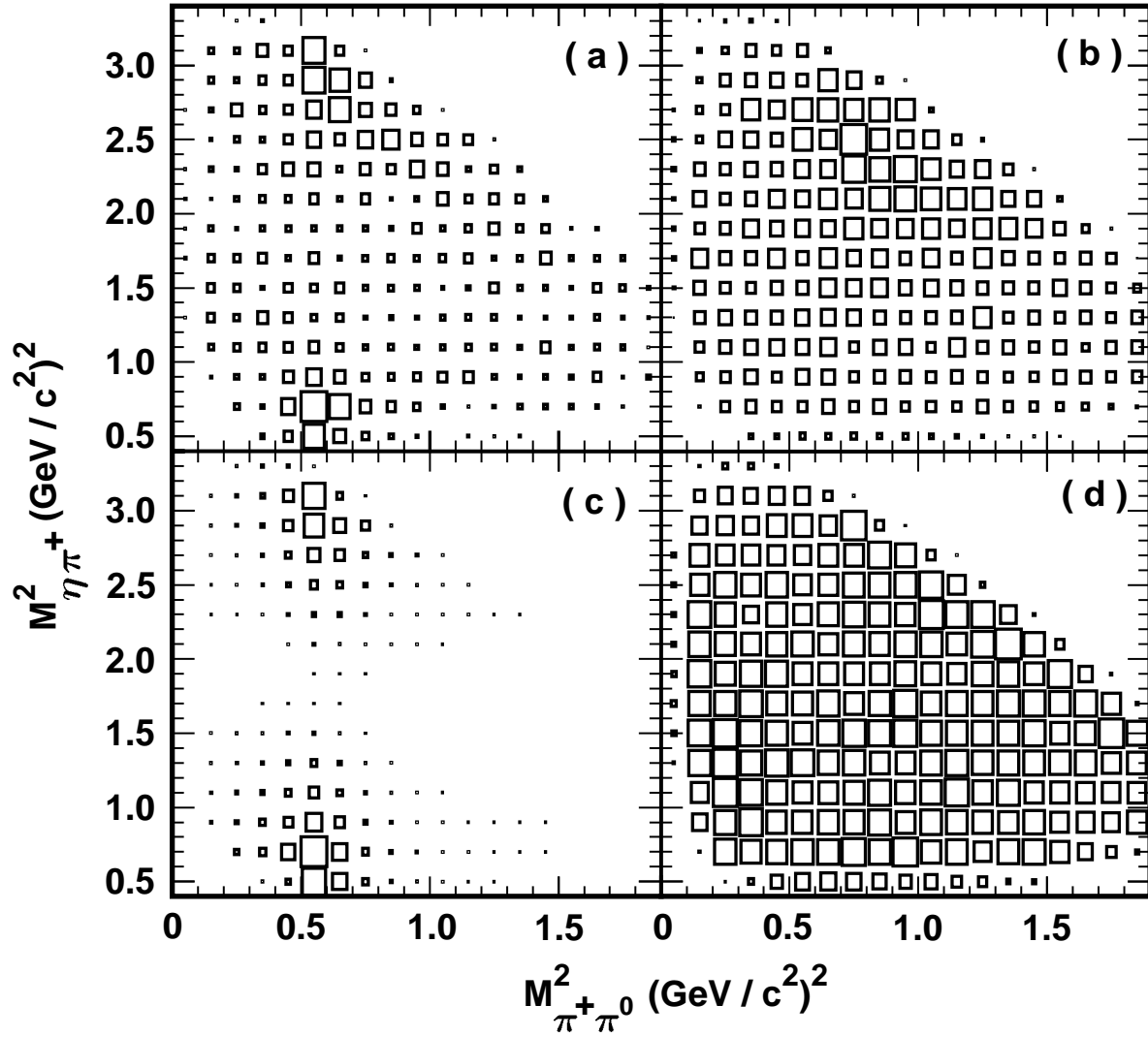


FIG. 7. Dalitz plot of $D_s^+ \rightarrow \eta \rho^+$, with $\eta \rightarrow \gamma \gamma$. The horizontal axis is $M_{\pi^+\pi^0}^2$; the vertical axis is $M_{\eta\pi^+}^2$. (a) Data signal region; (b) Data M_{D_s} sidebands; (c) MC signal; (d) MC simulation of nonresonant $\eta\pi^+\pi^0$, generated according to phase space.

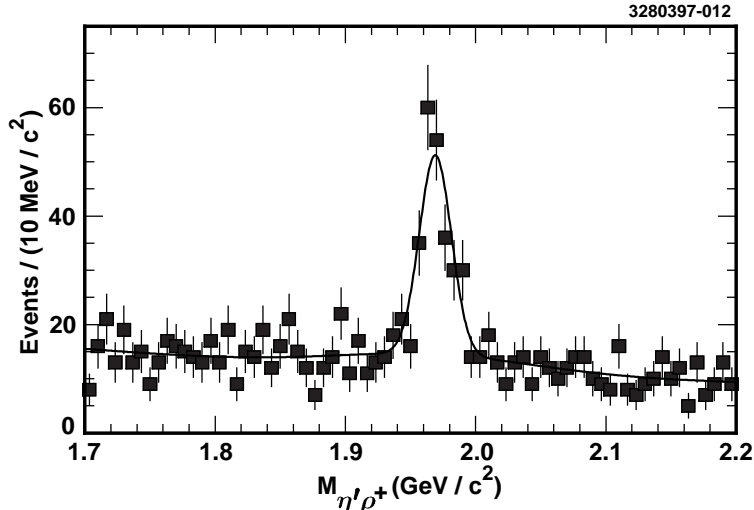


FIG. 8. The $M(\eta'\rho^+)$ distribution, with $\eta' \rightarrow \eta\pi^+\pi^-$, $\eta \rightarrow \gamma\gamma$.

signal from background, because the kinematic range for the di-pion mass does not extend beyond the region of the ρ . We do not expect $\eta'\pi$ resonant structures in this Dalitz plot because isospin forbids $s\bar{s} \rightarrow \eta'\pi$. We therefore fit the angular distribution alone to extract the ρ component. As for the case of the Dalitz fit for $\eta\rho^+$, we use three components in the fit: (a) the resonant signal shape, a fourth-order polynomial determined from the Monte Carlo, which includes the distortion of the pure $\cos^2\theta_{\pi^+}$ shape due to detector acceptance; (b) a nonresonant D_s^+ shape, which is linear; and (c) a non- D_s^+ background shape, which is a first-order polynomial determined by fitting the sidebands. As in the Dalitz fit, we fix the background normalization from the D_s^+ mass fit, and vary the normalizations of the signal and nonresonant parts.

Figure 9 shows the fit of the helicity angle distribution for the events in the D_s^+ mass peak. The results of the fit are shown in Table III. The total systematic error of 11% includes uncertainties in the photon detection efficiency (10%) and in the signal (4%), background (3%), and nonresonant (2%) shapes.

TABLE III. Fit Results for $D_s^+ \rightarrow (\eta, \eta')\rho^+$.

Mode	N	$\epsilon(\%)$	$\epsilon B(\%)$	$\Gamma/\Gamma(\phi\pi)$
$\phi\pi^+$	3000 ± 81	19.1 ± 0.2	9.4	
$\eta\rho^+$	447 ± 31	1.82 ± 0.07	0.47	$2.98 \pm 0.20 \pm 0.39$
$\eta'\rho^+$	137 ± 14	1.36 ± 0.04	0.15	$2.78 \pm 0.28 \pm 0.30$

The yields and upper limits on the branching ratios for the D^+ decays into final states with a ρ^+ are shown in Table IV.

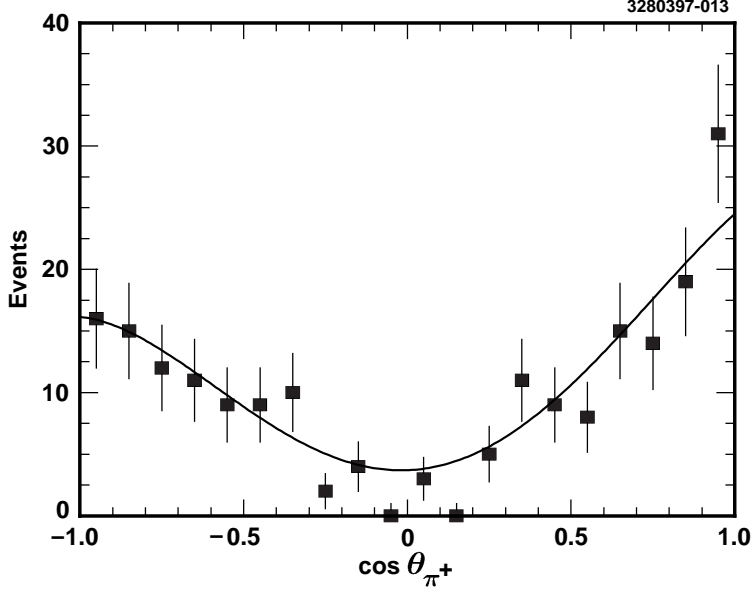


FIG. 9. The helicity angle distribution for events in the D_s^+ mass peak for the decay channel $D_s^+ \rightarrow \eta' \rho^+$.

TABLE IV. Fit Results for $D^+ \rightarrow (\eta, \eta') \rho^+$.

Type	N	$\epsilon(\%)$	$\epsilon B(\%)$	$\Gamma/\Gamma(\phi\pi)(90\%C.L)$
$\phi\pi^+$	970 ± 65	20.3 ± 0.2	9.9	
$\eta\rho^+$	8 ± 32	2.1 ± 0.1	0.55	<1.11
$\eta'\rho^+$	-4 ± 10	1.7 ± 0.1	0.19	<0.86

V. CONCLUSIONS

We have measured with improved statistics the branching ratios of the two-body hadronic decays of the D_s^+ : $D_s^+ \rightarrow \eta\pi^+$, $\eta'\pi^+$, $\eta\rho^+$, and $\eta'\rho^+$. The results are consistent with the previous CLEO measurements [4] and have improved errors. Using weighted averages of the two η modes, our results for $D_s^+ \rightarrow (\eta, \eta')\pi^+$ are:

$$\frac{\Gamma(D_s^+ \rightarrow \eta\pi^+)}{\Gamma(D_s^+ \rightarrow \phi\pi^+)} = 0.48 \pm 0.03 \pm 0.04$$

and

$$\frac{\Gamma(D_s^+ \rightarrow \eta'\pi^+)}{\Gamma(D_s^+ \rightarrow \phi\pi^+)} = 1.03 \pm 0.06 \pm 0.07.$$

The results for the ρ modes are:

$$\frac{\Gamma(D_s^+ \rightarrow \eta\rho^+)}{\Gamma(D_s^+ \rightarrow \phi\pi^+)} = 2.98 \pm 0.20 \pm 0.39$$

and

$$\frac{\Gamma(D_s^+ \rightarrow \eta'\rho^+)}{\Gamma(D_s^+ \rightarrow \phi\pi^+)} = 2.78 \pm 0.28 \pm 0.30.$$

Using these measurements and the published CLEO semileptonic measurements [5], we can calculate the ratios which test factorization: $\Gamma(D_s^+ \rightarrow \eta\rho^+)/\Gamma(D_s^+ \rightarrow \eta e^+\nu_e) = 4.4 \pm 1.2$ and $\Gamma(D_s^+ \rightarrow \eta'\rho^+)/\Gamma(D_s^+ \rightarrow \eta' e^+\nu_e) = 12.0 \pm 4.3$. The branching ratio for the mode $D_s^+ \rightarrow \eta'\rho^+$ is much larger than the value of 2.9 expected from factorization. Using the normalization $B(D_s^+ \rightarrow \phi\pi^+) = (3.6 \pm 0.9)\%$ [8], we calculate $B(D_s^+ \rightarrow \eta'\rho^+) = (10.0 \pm 1.5 \pm 2.5)\%$, where the second error is due to the uncertainty in the $D_s^+ \rightarrow \phi\pi^+$ branching fraction. This branching fraction is very large, considering the flavor wave function of the η' is only partly $s\bar{s}$ and that the rate is suppressed for such a P -wave decay very close to threshold. There is no obvious mechanism by which final state interactions could cause such a large enhancement of one of the dominant decay modes.

Table V summarizes the measurements of branching ratios for all four D_s^+ decays and compares them with theoretical calculations. Models which are successful in predicting other charm hadronic modes reasonably well predict $B(D_s^+ \rightarrow \eta'\rho^+)$ to be 1 – 3% [9–11]. This failure leads theorists to consider contributions to the amplitude from decay diagrams other than that shown in Figure 1. For example, Ball *et al.* [12] argue that the high branching ratio for $D_s^+ \rightarrow \eta'\rho$ could be due to a $c\bar{s}$ annihilation into a W^+ and two gluons, in which the two gluons hadronize as an η' .

TABLE V. Measurements and Predictions for Branching Ratios of D_s^+ Decays.

Mode	$\Gamma/\Gamma(\phi\pi^+)$	BSW [11]	HK [9]	BLP [10]
$\eta\pi$	0.48 ± 0.05	1.04	0.58 ± 0.15	0.30
$\eta\rho$	2.98 ± 0.44	1.96	2.86 ± 0.71	1.83
$\eta'\pi$	1.03 ± 0.09	0.61	1.55 ± 0.42	1.32
$\eta'\rho$	2.78 ± 0.41	0.55	$0.43^{+0.55}_{-0.32}$	0.59

Using the normalization $B(D^+ \rightarrow \phi\pi^+) = (6.1 \pm 0.6) \times 10^{-3}$ [8], we also calculate the D^+ branching fractions to the same final states. Table VI summarizes the results. Since the D^+ decays involve two diagrams which interfere, the theoretical calculations vary widely, and are expected to be somewhat less reliable than for the D_s^+ case.

TABLE VI. Measurements and Predictions for Branching Fractions of D^+ Decays. The experimental upper limits are at the 90% confidence level.

Mode	Branching Fraction (%)	BSW [11]	HK [9]	BLP [10]
$\eta\pi$	0.30 ± 0.06	0.004	0.68 ± 0.21	0.34
$\eta\rho$	< 0.68	0.06	< 0.48	0.01
$\eta'\pi$	0.50 ± 0.10	0.16	< 0.48	0.73
$\eta'\rho$	< 0.52	0.05	< 0.07	0.12

We gratefully acknowledge the effort of the CESR staff in providing us with excellent luminosity and running conditions. J.P.A., J.R.P., and I.P.J.S. thank the NYI program of the NSF, M.S. thanks the PFF program of the NSF, G.E. thanks the Heisenberg Foundation, K.K.G., M.S., H.N.N., T.S., and H.Y. thank the OJI program of DOE, J.R.P., K.H., M.S. and V.S. thank the A.P. Sloan Foundation, R.W. thanks the Alexander von Humboldt

Stiftung, and M.S. thanks Research Corporation for support. This work was supported by the National Science Foundation, the U.S. Department of Energy, and the Natural Sciences and Engineering Research Council of Canada.

REFERENCES

- [1] A.N. Kamal *et al.*, Phys. Rev. D**49**, 1330 (1994).
- [2] CLEO Collaboration, A. Bean *et al.*, Phys. Lett. B**317**, 647 (1993).
- [3] Note that the approximate equality of the two ratios is coincidental. See [1].
- [4] CLEO Collaboration, M. Daoudi *et al.*, Phys. Rev. D**45**, 3965 (1992). The branching ratios measured in that paper were: $\frac{\Gamma(D_s^+ \rightarrow \eta\pi^+)}{\Gamma(D_s^+ \rightarrow \phi\pi^+)} = 0.54 \pm 0.09 \pm 0.06$, $\frac{\Gamma(D_s^+ \rightarrow \eta'\pi^+)}{\Gamma(D_s^+ \rightarrow \phi\pi^+)} = 1.20 \pm 0.15 \pm 0.11$, $\frac{\Gamma(D_s^+ \rightarrow \eta\rho^+)}{\Gamma(D_s^+ \rightarrow \phi\pi^+)} = 2.86 \pm 0.38_{-0.38}^{+0.36}$, and $\frac{\Gamma(D_s^+ \rightarrow \eta'\rho^+)}{\Gamma(D_s^+ \rightarrow \phi\pi^+)} = 3.44 \pm 0.62_{-0.46}^{+0.44}$. The present paper includes the data used in the 1992 paper. Thus the new results should not be averaged with the old results.
- [5] CLEO Collaboration, G. Brandenburg *et al.*, Phys. Rev. Lett. **75**, 3804 (1995).
- [6] CLEO Collaboration, Y. Kubota *et al.*, Nucl. Instrum. Methods Phys. Res., Sect. A **320**, 66 (1992).
- [7] R. Brun *et al.* GEANT3, CERN DD/EE/84-1 (1987).
- [8] Particle Data Group, Phys. Rev. D **54**, 1(1996).
- [9] I. Hinchliffe and T.A. Kaeding, Phys. Rev. D**54**, 914 (1996).
- [10] F. Buccella, M. Lusignoli, and A. Pugliese, Phys. Lett. B**379**, 249(1996).
- [11] M. Bauer, B. Stech, and M. Wirbel, Z. Phys. C **34**, 102(1987).
- [12] P. Ball, J.M. Frere, and M. Tytgat, Phys. Lett. B**365**, 367(1996).